Nonlinear Legendre Spectral Finite Elements for Wind Turbine Blade Dynamics[*]

Qi Wang[†1], Michael A. Sprague[‡1], Jason Jonkman[§1] and Nick Johnson[¶2]

[1]National Renewable Energy Laboratory, Golden, CO 80401
[2]Colorado School of Mines, Golden, CO 80401

This paper presents a numerical implementation and evaluation of a new nonlinear beam finite element model appropriate for highly flexible wind turbine blades made of composite materials. The underlying model uses the geometrically exact beam theory (GEBT) and spatial discretization is accomplished with Legendre spectral finite elements (LSFEs). The displacement-based GEBT is presented, which includes the coupling effects that exist in composite structures with geometric nonlinearity. LSFEs are high-order finite elements with nodes located at the Gauss-Legendre-Lobatto points. LSFEs can be an order of magnitude more efficient that low-order finite elements for a given accuracy level. The LSFE code is implemented in the software module called BeamDyn in the new FAST modularization framework for dynamic simulation of highly flexible composite-material wind turbine blades. The framework allows for simulations of wind turbines in operating conditions. In this paper, we verify BeamDyn for static and dynamic nonlinear deformation of composite beams and compare BeamDyn LSFE performance against common low-order finite elements found in a commercial code. Comparisons show that the BeamDyn LSFEs can provide dramatically more accurate results for a given model size.

I.   Introduction

Wind power is becoming one of the most important renewable-energy sources in the United States. In recent years, the size of wind turbines has been increasing to lower the cost, which leads to highly flexible turbine blades. These huge electro-mechanical systems pose a significant challenge for engineering design and analysis. Although possible with modern super computers, direct three-dimensional (3D) structural analysis is so computationally expensive that the wind industry is always seeking efficient high-fidelity engineering models.

Beam models are widely used to represent and analyze engineering structures that have one of its dimensions much larger than the other two. Many engineering components can be idealized as beams: bridges in civil engineering, joists and lever arms in heavy-machine industries, and helicopter rotor blades. The blades, tower, and shaft in a wind turbine system are well suited to idealization as beams. In the weight-critical applications of beam structures, like high-aspect-ratio wings in aerospace and wind energy, composite materials are attractive due to their superior strength-to-weight and stiffness-to-weight ratios. However, analysis of composite-materials structures is more difficult than their isotropic counterparts due to elastic-coupling effects. The geometrically exact beam theory (GEBT), first proposed by Reissner[1], is a method that has proven powerful for analysis of highly flexible composite beams in the helicopter engineering community. During the past several decades, much effort has been invested in this area. Simo[2] and Simo and Vu-Quoc[3] extended Reissner's work to deal with 3D dynamic problems. Jelenić and Crisfield[4] implemented this theory using the finite-element (FE) method where a new approach for interpolating the rotation field was proposed that preserves the geometric exactness. Betsch and Steinmann[5] circumvented the interpolation of rotation by introducing a re-parameterization of the weak form corresponding to the equations of motion. It is noted that Ibrahimbegović and his colleagues implemented this theory for static[6] and dynamic[7] analysis. In contrast to the displacement-based implementations, the geometrically exact beam theory has also been formulated by mixed finite elements where both the primary and dual fields are independently interpolated. In the mixed formulation, all of the necessary ingredients, including Hamilton's principle and kinematic equations, are combined in a single variational-formulation statement; Lagrange multipliers, motion variables, generalized strains, forces and moments, linear and angular momenta, and displacement and rotation variables are considered as independent quantities. Yu et al.[8] and Wang et al.[9] presented

---

[†]Research Engineer, National Wind Technology Center, AIAA Member. Email: Qi.Wang2@nrel.gov
[‡]Senior Research Scientist, Scientific Computing Center, AIAA Member. Email: Michael.A.Sprague@nrel.gov
[§]Senior Engineer, National Wind Technology Center, AIAA Member. Email: Jason.Jonkman@nrel.gov.
[¶]Graduate Research Assistant, Department of Mechanical Engineering.

American Institute of Aeronautics and Astronautics

the implementation of GEBT in a mixed formulation; various rotation parameters were investigated and the code was validated against analytical and numerical solutions. Readers are referred to Hodges[10], where comprehensive derivations and discussions on nonlinear composite-beam theories can be found.

Legendre spectral finite elements[11,12] (LSFEs) are p-type elements whose shape functions are Lagrangian interpolants with node locations at the Gauss-Lobatto-Legendre (GLL) points. LSFEs combine the accuracy of global spectral methods with the geometric-modeling flexibility of h-type FEs. LSFEs have seen successful use in the simulation of fluid dynamics[11–13], two-dimensional elastic wave propagation in solid media in geophysics[14], elastodynamics[15], and acoustic wave propagation[16]. LSFEs have been applied to the linear-response analysis of beams[17–21] and plate elements[22–24]. Xiao and Zhong[25] reported a displacement-based implementation by LSFEs for two-dimensional static nonlinear beam deformation. Their LSFEs were compared against a mixed-formulation low-order-FE GEBT code by Wang and Sprague[21]; it was shown that the LSFEs provide exponential convergence rates, while the low-order FEs were limited to an algebraic convergence rate.

In this paper, we present a three-dimensional displacement-based implementation of the geometrically exact beam theory using LSFEs. This work builds on previous efforts that showed the implementation of 3D rotation parameters[9] and a demonstration example of two-dimensional nonlinear spectral beam elements[21] for static deformation. The code implemented in this work is in accordance with the new FAST modularization framework[26], which allows coupled aero-hydro-servo-elastic simulation of both land-based and offshore wind turbine under realistic operating conditions. The goal is to complete the coupled code by June 2014.

The paper is organized as follows. The theoretical foundation of the geometrically exact beam theory is introduced first. Then the spatial discretization by LSFEs is discussed. Finally, verification examples are provided to show the accuracy and efficiency of the present model for composite beams.

II. Geometrically Exact Beam Theory

For completeness, this section reviews the geometrically exact beam theory and linearization process of the governing equations. The content of this section can be found in other papers and textbooks (see, e.g., Bauchau[27]) Figure 1 shows a beam in its initial undeformed and deformed states. A reference frame $\mathbf{b}_i$, for $i = \{1, 2, 3\}$, is introduced along the beam axis for the undeformed state; a frame $\mathbf{B}_i$ is introduced along each point of the deformed beam axis. Curvilinear-coordinate x_1 defines the intrinsic parameterization of the reference line; similarly, s denotes the deformed reference line. It is noted that the unit vector $\mathbf{B}_1$ is not necessarily tangent to the deformed reference line $\mathbf{R}$ unless one adopts the Euler-Bernoulli hypothesis.
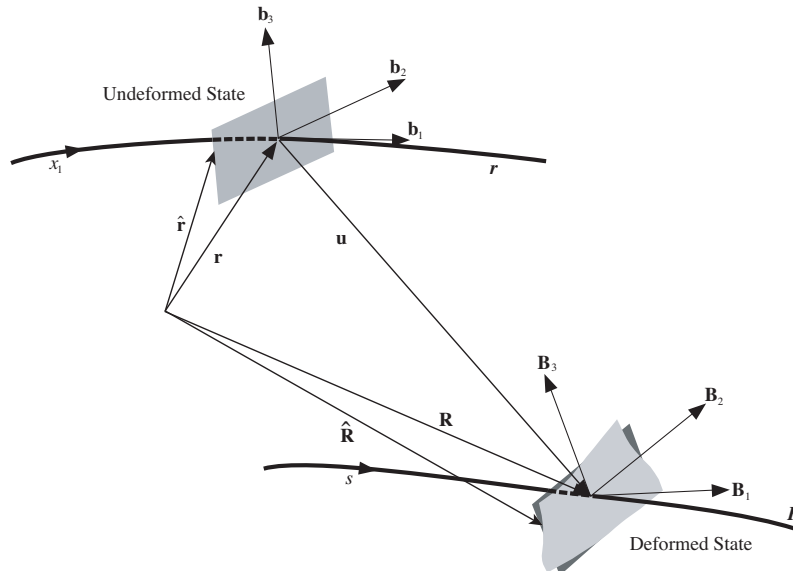

Figure 1: Schematic of a beam segment in its undeformed state (i.e., reference configuration) and its deformed state (current configuration) with associated kinematic variables.

In this paper, we use matrix notation to denote vectorial or vectorial-like quantities. For example, we use an underline to denote a vector $\underline{u}$, a bar to denote unit vector $\bar{n}$, and double underline to denote a tensor $\underline{\underline{\Delta}}$. Note that sometimes the underlines only denote the dimension of the corresponding matrix. The governing equations of motion

American Institute of Aeronautics and Astronautics

for geometrically exact beam theory can be written as[27]

$$\dot{\underline{h}} - \underline{F}' = \underline{f} \tag{1}$$

$$\dot{\underline{g}} + \dot{\tilde{\underline{u}}}\underline{h} - \underline{M}' - (\tilde{x}'_0 + \tilde{u}')\underline{F} = \underline{m} \tag{2}$$

where $\underline{h}$ and $\underline{g}$ are the linear and angular momenta resolved in the reference coordinate system, respectively; $\underline{F}$ and $\underline{M}$ are the beam's sectional forces and moments, respectively; $\underline{u}$ is the displacement of the reference line; $\underline{x}_0$ is the initial position vector of a point along the beam's reference line; $\underline{f}$ and $\underline{m}$ are the distributed force and moment applied to the beam structure. A prime indicates a derivative with respect to the beam axis x_1 and an overdot indicates a derivative with respect to time. The tilde operator, i.e., $(\tilde{\cdot})$, denotes a second-order, skew-symmetric tensor corresponding to the given vector. In the literature, it is also termed as a "cross-product matrix". For example, for the vector $\overline{n}$,

$$\widetilde{n} = \begin{bmatrix} 0 & -n_3 & n_2 \\ n_3 & 0 & -n_1 \\ -n_2 & n_1 & 0 \end{bmatrix}$$

The constitutive equations relate the velocities to the momenta and the one-dimensional strain measures to the sectional resultants as

$$\begin{Bmatrix} \underline{h} \\ \underline{g} \end{Bmatrix} = \underline{\underline{\mathcal{M}}} \begin{Bmatrix} \dot{\underline{u}} \\ \underline{\omega} \end{Bmatrix} \tag{3}$$

$$\begin{Bmatrix} \underline{F} \\ \underline{M} \end{Bmatrix} = \underline{\underline{\mathcal{C}}} \begin{Bmatrix} \underline{\epsilon} \\ \underline{\kappa} \end{Bmatrix} \tag{4}$$

where $\underline{\underline{\mathcal{M}}}$ and $\underline{\underline{\mathcal{C}}}$ are the 6×6 sectional mass and stiffness matrices resolved in the inertial basis, respectively (note that they are not tensors); $\underline{\epsilon}$ and $\underline{\kappa}$ are the one-dimensional (1D) strains and curvatures, respectively; $\underline{\omega}$ is the angular velocity vector that is defined by the rotation tensor $\underline{\underline{R}}$ as $\underline{\omega} = \mathrm{axial}(\dot{\underline{\underline{R}}}\,\underline{\underline{R}})$. The 1D strain measures are defined as

$$\begin{Bmatrix} \underline{\epsilon} \\ \underline{\kappa} \end{Bmatrix} = \begin{Bmatrix} \underline{x}'_0 + \underline{u}' - (\underline{\underline{R}}\,\underline{\underline{R}}_0)\overline{\imath}_1 \\ \underline{k} + \underline{\underline{R}}\,\underline{k}_i \end{Bmatrix} \tag{5}$$

where $\underline{k} = \mathrm{axial}(\underline{\underline{R}}'\underline{\underline{R}}^T)$ is the sectional curvature vector resolved in the inertial basis, $\underline{k}_i$ is the corresponding initial curvature vector, and $\overline{\imath}_1$ is the unit vector along x_1 direction in the inertial basis.

For a displacement-based finite element implementation, there are six degree-of-freedoms at each node: three displacement components and three rotation components. Here we use $\underline{q}$ to denote the elemental displacement array as $\underline{q} = \begin{bmatrix} \underline{u}^T & \underline{p}^T \end{bmatrix}$ where $\underline{u}$ is the displacement and $\underline{p}$ is the rotation-parameter vector. The acceleration array can thus be defined as $\underline{a} = \begin{bmatrix} \ddot{\underline{u}}^T & \dot{\underline{\omega}}^T \end{bmatrix}$. For nonlinear finite-element analysis, the discretized and incremental forms of displacement, velocity, and acceleration are written as

$$\underline{q}(x_1) = \underline{\underline{N}}\,\hat{\underline{q}} \quad \Delta\underline{q}^T = \begin{bmatrix} \Delta\underline{u}^T & \Delta\underline{p}^T \end{bmatrix} \tag{6}$$

$$\underline{v}(x_1) = \underline{\underline{N}}\,\hat{\underline{v}} \quad \Delta\underline{v}^T = \begin{bmatrix} \Delta\dot{\underline{u}}^T & \Delta\underline{\omega}^T \end{bmatrix} \tag{7}$$

$$\underline{a}(x_1) = \underline{\underline{N}}\,\hat{\underline{a}} \quad \Delta\underline{a}^T = \begin{bmatrix} \Delta\ddot{\underline{u}}^T & \Delta\dot{\underline{\omega}}^T \end{bmatrix} \tag{8}$$

where $\underline{\underline{N}}$ is the shape function matrix and $(\hat{\cdot})$ denotes a column matrix of nodal values. It is noted that given the "untensorial" nature, we need to adopt a special algorithm to deal with the 3D rotations, which will be introduced in the next section. The governing equations for beams are highly nonlinear; a linearization process is needed if a Newton-Raphson nonlinear solver is to be used for static analysis and dynamic analysis, for which an implicit time integration scheme is adopted. According to Bauchau[27], the linearized governing equations in Eq. (1) and (2) are in the form of

$$\underline{\underline{\hat{M}}}\Delta\hat{\underline{a}} + \underline{\underline{\hat{G}}}\Delta\hat{\underline{v}} + \underline{\underline{\hat{K}}}\Delta\hat{\underline{q}} = \hat{\underline{F}}^{ext} - \hat{\underline{F}} \tag{9}$$

where the $\underline{\underline{\hat{M}}}$, $\underline{\underline{\hat{G}}}$, and $\underline{\underline{\hat{K}}}$ are the elemental mass, gyroscopic, and stiffness matrices, respectively; $\hat{\underline{F}}$ and $\hat{\underline{F}}^{ext}$ are the elemental forces and externally applied loads, respectively. They are defined for an element of length l along x_1 as

American Institute of Aeronautics and Astronautics

follows

$$\underline{\hat{M}} = \int_0^l \underline{N}^T \underline{\underline{M}} \, \underline{N} dx_1 \tag{10}$$

$$\underline{\hat{G}} = \int_0^l \underline{N}^T \underline{\underline{G}}^I \, \underline{N} dx_1 \tag{11}$$

$$\underline{\hat{K}} = \int_0^l \left[\underline{N}^T (\underline{\underline{K}}^I + \underline{\underline{Q}}) \, \underline{N} + \underline{N}^T \underline{\underline{P}} \, \underline{N}' + \underline{N}'^T \underline{\underline{C}} \, \underline{N}' + \underline{N}'^T \underline{\underline{O}} \, \underline{N} \right] dx_1 \tag{12}$$

$$\underline{\hat{F}} = \int_0^l (\underline{N}^T \underline{\mathcal{F}}^I + \underline{N}^T \underline{\mathcal{F}}^D + \underline{N}'^T \underline{\mathcal{F}}^C) dx_1 \tag{13}$$

$$\underline{\hat{F}}^{ext} = \int_0^l \underline{N}^T \underline{\mathcal{F}}^{ext} dx_1 \tag{14}$$

where $\underline{\mathcal{F}}^{ext}$ is the applied load vector. The new matrix notations in Eqs. (10) to (14) are briefly introduced here. $\underline{\mathcal{F}}^C$ and $\underline{\mathcal{F}}^D$ are elastic forces obtained from Eq. (1) and (2) as

$$\underline{\mathcal{F}}^C = \left\{ \begin{matrix} \underline{F} \\ \underline{M} \end{matrix} \right\} = \underline{\underline{C}} \left\{ \begin{matrix} \underline{\epsilon} \\ \underline{\kappa} \end{matrix} \right\} \tag{15}$$

$$\underline{\mathcal{F}}^D = \left[\begin{matrix} \underline{0} & \underline{0} \\ (\tilde{x}_0' + \tilde{u}')^T & \underline{0} \end{matrix} \right] \underline{\mathcal{F}}^C \equiv \underline{\underline{\Upsilon}} \, \underline{\mathcal{F}}^C \tag{16}$$

where $\underline{0}$ denotes a 3×3 null matrix. The $\underline{\underline{G}}^I, \underline{\underline{K}}^I, \underline{\underline{O}}, \underline{\underline{P}}, \underline{\underline{Q}}$, and $\underline{\mathcal{F}}^I$ in Eq. (11), Eq. (12), and Eq. (13) are defined as

$$\underline{\underline{G}}^I = \left[\begin{matrix} \underline{0} & (\widetilde{\tilde{\omega}m\eta})^T + \tilde{\omega}m\tilde{\eta}^T \\ \underline{0} & \tilde{\omega}\underline{\underline{\varrho}} - \underline{\underline{\varrho}}\widetilde{\omega} \end{matrix} \right] \tag{17}$$

$$\underline{\underline{K}}^I = \left[\begin{matrix} \underline{0} & \dot{\tilde{\omega}}m\tilde{\eta}^T + \tilde{\omega}\tilde{\omega}m\tilde{\eta}^T \\ \underline{0} & \ddot{\tilde{u}}m\tilde{\eta} + \underline{\underline{\varrho}}\dot{\tilde{\omega}} - \underline{\underline{\varrho}}\widetilde{\dot{\omega}} + \tilde{\omega}\underline{\underline{\varrho}}\tilde{\omega} - \tilde{\omega}\underline{\underline{\varrho}}\widetilde{\omega} \end{matrix} \right] \tag{18}$$

$$\underline{\underline{O}} = \left[\begin{matrix} \underline{0} & \underline{\underline{C}}_{11}\tilde{E}_1 - \tilde{F} \\ \underline{0} & \underline{\underline{C}}_{21}\tilde{E}_1 - \tilde{M} \end{matrix} \right] \tag{19}$$

$$\underline{\underline{P}} = \left[\begin{matrix} \underline{0} & \underline{0} \\ \tilde{F} + (\underline{\underline{C}}_{11}\tilde{E}_1)^T & (\underline{\underline{C}}_{21}\tilde{E}_1)^T \end{matrix} \right] \tag{20}$$

$$\underline{\underline{Q}} = \underline{\underline{\Upsilon}} \, \underline{\underline{O}} \tag{21}$$

$$\underline{\mathcal{F}}^I = \left\{ \begin{matrix} m\ddot{\underline{u}} + (\dot{\tilde{\omega}} + \tilde{\omega}\tilde{\omega})m\eta \\ m\tilde{\eta}\ddot{\underline{u}} + \underline{\underline{\varrho}}\dot{\omega} + \tilde{\omega}\underline{\underline{\varrho}}\omega \end{matrix} \right\} \tag{22}$$

where m is the mass density per unit length, $\underline{\eta}$ is the location of the sectional center of mass, $\underline{\underline{\varrho}}$ is the moment of inertia tensor, and the following notations were introduced to simplify the above expressions

$$\underline{E}_1 = \underline{x}_0' + \underline{u}' \tag{23}$$

$$\underline{\underline{C}} = \left[\begin{matrix} \underline{\underline{C}}_{11} & \underline{\underline{C}}_{12} \\ \underline{\underline{C}}_{21} & \underline{\underline{C}}_{22} \end{matrix} \right] \tag{24}$$

It is noted that the 3D rotations are represented as Wiener-Milenković parameters [9,28] defined in the following equation:

$$\underline{p} = 4\tan\left(\frac{\phi}{4}\right)\bar{n} \tag{25}$$

where ϕ is the rotation angle and $\bar{n}$ is the unit vector of the rotation axis. It can be observed that the valid range for this parameter is $|\phi| < 2\pi$. The singularities existing at integer multiples of $\pm 2\pi$ can be removed by a rescaling operation at π, as given in Bauchau et al. [28]:

$$\underline{r} = \begin{cases} 4(q_0\underline{p} + p_0\underline{q} + \tilde{p}\underline{q})/(\Delta_1 + \Delta_2), & \text{if } \Delta_2 \geq 0 \\ -4(q_0\underline{p} + p_0\underline{q} + \tilde{p}\underline{q})/(\Delta_1 - \Delta_2), & \text{if } \Delta_2 < 0 \end{cases} \tag{26}$$

where $\underline{p}$, $\underline{q}$, and $\underline{r}$ are the vectorial parameterization of three finite rotations such that $\underline{R}(\underline{r}) = \underline{R}(\underline{p})\underline{R}(\underline{q})$, $p_0 = 2 - \underline{p}^T\underline{p}/8$, $q_0 = 2 - \underline{q}^T\underline{q}/8$, $\Delta_1 = (4 - p_0)(4 - q_0)$, and $\Delta_2 = p_0 q_0 - \underline{p}^T\underline{q}$. It is noted that the rescaling operation could cause a discontinuity of the interpolated rotation field; therefore a more robust interpolation algorithm will be introduced in the next section where the rescaling-independent relative-rotation field is interpolated.

III.   Numerical Implementation with Legendre Spectral Finite Elements

The displacement fields in an element are approximated as

$$\underline{u}(\xi) = \sum_{k=1}^{p+1} h^k(\xi)\underline{\hat{u}}^k \tag{27}$$

$$\underline{u}'(\xi) = \sum_{k=1}^{p+1} h^{k\prime}(\xi)\underline{\hat{u}}^k \tag{28}$$

where $h^k(\xi)$, the component of shape function matrix $\underline{N}$, is the pth-order polynomial Lagrangian-interpolant shape function of node k, $k = \{1, 2, ..., p+1\}$, $\underline{\hat{u}}^k$ is the kth nodal value, and $\xi \in [-1, 1]$ is the element natural coordinate. However, as discussed in Bauchau et al.[28], the 3D rotation field cannot simply be interpolated as the displacement field in the form of

$$\underline{c}(\xi) = \sum_{k=1}^{p+1} h^k(\xi)\underline{\hat{c}}^k \tag{29}$$

$$\underline{c}'(\xi) = \sum_{k=1}^{p+1} h^{k\prime}(\xi)\underline{\hat{c}}^k \tag{30}$$

where $\underline{c}$ is the rotation field in an element and $\underline{\hat{c}}^k$ is the nodal value at the kth node, for three reasons: 1) rotations do not form a linear space so that they must be "composed" rather than added; 2) a rescaling operation is needed to eliminate the singularity existing in the vectorial rotation parameters; 3) the rotation field lacks objectivity, which, as defined by Jelenić and Crisfield[4], refers to the invariance of strain measures computed through interpolation to the addition of a rigid-body motion. Therefore, we adopt the more robust interpolation approach proposed by Jelenić and Crisfield[4] to deal with the finite rotations. Our approach is described as follows

Step 1: Compute the nodal relative rotations, $\underline{\hat{r}}^k$, by removing the reference rotation, $\underline{\hat{c}}^1$, from the finite rotation at each node, $\underline{\hat{r}}^k = (\underline{\hat{c}}^{1-}) \oplus \underline{\hat{c}}^k$. It is noted that the minus sign on $\underline{\hat{c}}^1$ denotes that the relative rotation is calculated by removing the reference rotation from each node. The composition in that equation is an equivalent of $\underline{R}(\underline{\hat{r}}^k) = \underline{R}^T(\underline{\hat{c}}^1) \, \underline{R}(\underline{c}^k)$.

Step 2: Interpolate the relative-rotation field: $\underline{r}(\xi) = h^k(\xi)\underline{\hat{r}}^k$ and $\underline{r}'(\xi) = h^{k\prime}(\xi)\underline{\hat{r}}^k$. Find the curvature field $\underline{\kappa}(\xi) = \underline{R}(\underline{\hat{c}}^1)\underline{H}(r)\underline{r}'$, where $\underline{H}$ is the tangent tensor that relates the curvature vector $\underline{k}$ and rotation vector $\underline{p}$ as

$$\underline{k} = \underline{H} \, \underline{p}' \tag{31}$$

Step 3: Restore the rigid-body rotation removed in Step 1: $\underline{c}(\xi) = \underline{\hat{c}}^1 \oplus \underline{r}(\xi)$.

Note that the relative-rotation field can be computed with respect to any of the nodes of the element; we choose node 1 as the reference node for convenience. In the LSFE approach, shape functions (i.e., those composing $\underline{N}$) are p^{th}-order Lagrangian interpolants, where nodes are located at the $p+1$ GLL-quadrature points in the $[-1, 1]$ element natural-coordinate domain. Figure 2 shows representative LSFE basis functions for fourth- and eighth-order elements. Note that nodes are clustered near element endpoints. In the present implementation, weak-form integrals are evaluated with p-point reduced Gauss quadrature.
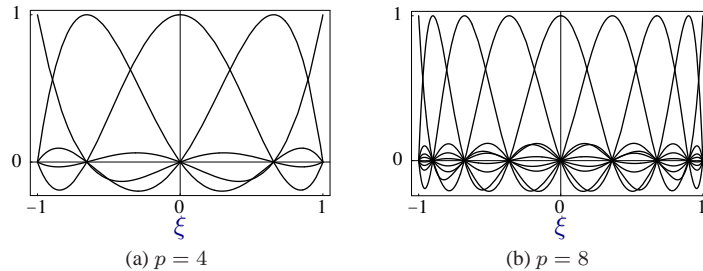

(a) $p = 4$ (b) $p = 8$

Figure 2: Representative $p+1$ Lagrangian-interpolant shape functions in the element natural coordinates for (a) fourth- and (b) eighth-order LSFEs, where nodes are located at the Gauss-Lobatto-Legendre points.

The geometrically exact beam theory has been implemented with LSFEs in a code called BeamDyn, which is a new module of FAST for wind turbine analysis. The system of nonlinear equations in Eqs. (1) and (2) are solved using the Newton-Raphson method with the linearized form in Eq. (9). In the present implementation, an energy-like stopping criterion has been chosen, which is calculated as

$$\|\Delta \mathbf{U}^{(i)T}\left(^{t+\Delta t}\mathbf{R} - {}^{t+\Delta t}\mathbf{F}^{(i-1)}\right)\| \leq \|\epsilon_E\left(\Delta \mathbf{U}^{(1)T}\left(^{t+\Delta t}\mathbf{R} - {}^{t}\mathbf{F}\right)\right)\| \tag{32}$$

where $\|\cdot\|$ denotes the Euclidean norm, $\Delta \mathbf{U}$ is the incremental displacement vector, $\mathbf{R}$ is the vector of externally applied nodal point loads, $\mathbf{F}$ is the vector of nodal point forces corresponding to the internal element stresses, and ϵ_E is the preset energy tolerance. The superscript on the left side of a variable denotes the time-step number (in a dynamic analysis), while the one on the right side denotes the Newton-Raphson iteration number. As pointed out by Bathe and Cimento[29], this criterion provides a measure of when both the displacements and the forces are near their equilibrium values. Time integration is performed using the generalized-α scheme in BeamDyn, which is an unconditionally stable (for linear systems), second-order accurate algorithm. The scheme allows for users to choose integration parameters that introduce high-frequency numerical dissipation. More details regarding the generalized-α method can be found in Refs.[27,30].

IV. Numerical Examples

A. Example 1: Static bending of a cantilever beam

The first example is a common benchmark problem for geometrically nonlinear analysis of beams[2,25]. We calculate the static deflection of a cantilever beam that is subjected at its free end to a constant moment about the x_2 axis, M_2; a system schematic is shown in Figure 3. The length of the beam L is 10 inches and the cross-sectional stiffness matrix is

$$C^* = 10^3 \times \begin{bmatrix} 1770 & 0 & 0 & 0 & 0 & 0 \\ 0 & 1770 & 0 & 0 & 0 & 0 \\ 0 & 0 & 1770 & 0 & 0 & 0 \\ 0 & 0 & 0 & 8.16 & 0 & 0 \\ 0 & 0 & 0 & 0 & 86.9 & 0 \\ 0 & 0 & 0 & 0 & 0 & 215 \end{bmatrix} \tag{33}$$

which has units of C_{ij}^* (lb), $C_{i,j+3}^*$ (lb.in), and $C_{i+3,j+3}^*$ (lb.in^2) for $i,j = 1,2,3$; these units are adopted for consistency with those used in Ref.[33] in this paper and apply to all subsequent stiffness matrices. It is pointed out that the term with an asterisk denotes that it is resolved in the material basis and the sectional stiffness matrix $\underline{C}$ resolved in the inertial basis can be obtained by $\underline{C} = (\underline{\underline{R}}\,\underline{\underline{R}}_0)\underline{C}^*(\underline{\underline{R}}\,\underline{\underline{R}}_0)^T$, where $\underline{\underline{R}}$ and $\underline{\underline{R}}_0$ denote the rotation matrix and the corresponding initial rotation matrix, respectively.
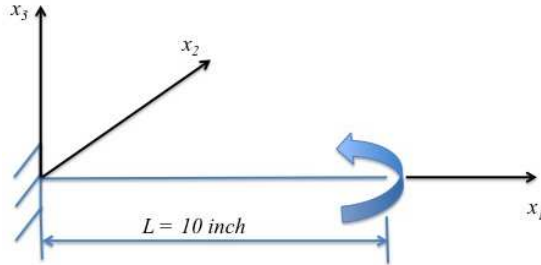

Figure 3: Schematic of a cantilever beam with tip moment, which was used in BeamDyn verification and performance studies.

The load applied at the tip about the negative x_2 direction is given by

$$M_2 = \lambda \bar{M}_2 \tag{34}$$

where $\bar{M}_2 = \pi \frac{EI_2}{L}$; and the parameter λ will vary between 0 and 2. In this case, the beam is discretized with two 5th-order LSFEs. It is noted that the maximum relative rotation in a single element cannot be greater than π as described in Ref.[28] in the current parameterization of 3D rotations, which is why two elements are needed. The static deformations of the beam obtained from BeamDyn are shown in Figure 4 for six different tip moments. The calculated tip displacements are compared with the analytical solution in Table 1, which can be found in Mayo et al.[31] as

$$u_1 = \rho \sin\left(\frac{x_1}{\rho}\right) - x_1 \quad u_3 = \rho\left(1 - \cos\left(\frac{x_1}{\rho}\right)\right) \tag{35}$$

American Institute of Aeronautics and Astronautics

Table 1: Comparison of analytical and BeamDyn-calculated tip displacements u_1 and u_3 (in inches) of a cantilever beam subjected to a constant moment; the BeamDyn model was composed of two 5th-order LSFEs.

λ	Analytical (u_1)	BeamDyn (u_1)	Analytical (u_3)	BeamDyn (u_3)
0.4	-2.4317	-2.4317	5.4987	5.4987
0.8	-7.6613	-7.6613	7.1978	7.1979
1.2	-11.5591	-11.5591	4.7986	4.7986
1.6	-11.8921	-11.8921	1.3747	1.3747
2.0	-10.0000	-10.0000	0.0000	0.0000

where $\rho = \frac{EI_2}{M_2}$. At this discretization level, BeamDyn results are virtually identical to those of the analytical solution.
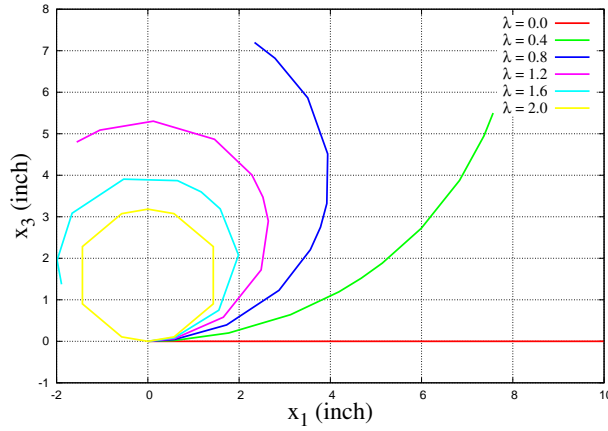
Figure 4: Static deflection of a cantilever beam under six constant bending moments as calculated with two 5th-order Legendre spectral FEs in BeamDyn.

The rotation parameter p_2 and rotation angle ϕ_2 at each node along beam axis x_1 obtained from BeamDyn are plotted in Figure 5a for $\lambda = 0.8$ and $\lambda = 2.0$, respectively. A rescaling can be observed from this figure for the case $\lambda = 2.0$. It is noted that although the rotation parameters are not continuous between elements due to the rescaling operation, the relative rotations are continuous in a single element as described in the previous section, which can be observed in Figure 5b.

Finally, we conduct a convergence study of the BeamDyn LSFEs. The convergence rate is compared with conventional quadratic elements used in Dymore[32], which is a well-known FE based multibody dynamics code for the comprehensive modeling of flexible multibody systems. For each test case, BeamDyn and Dymore have approximately the same number of Newton-Raphson iterations. Figure 6 shows the normalized error $\varepsilon(u)$, where u is the calculated tip displacement (at $x = L$), as a function of the number of model nodes for the calculation with Dymore quadratic finite elements (QFE) and a single LSFE, where

$$\varepsilon(u) = \left| \frac{u - u^a}{u^a} \right| \tag{36}$$

and where u^a is the analytical solution. The parameter λ is set to 1.0 for this case. The LSFEs (with p-refinement) exhibit highly desirable exponential convergence to machine-precision error, whereas the conventional quadratic elements are limited to algebraic convergence. Here, for a given model size, an LSFE model can be orders of magnitude more accurate than its QFE counterpart.

B. Example 2: Static analysis of a composite beam

The second example is to show the capability of BeamDyn for composite beams with elastic coupling. The cantilever beam used in this case is 10 inches long with a boxed cross-section made of composite materials that can be found in
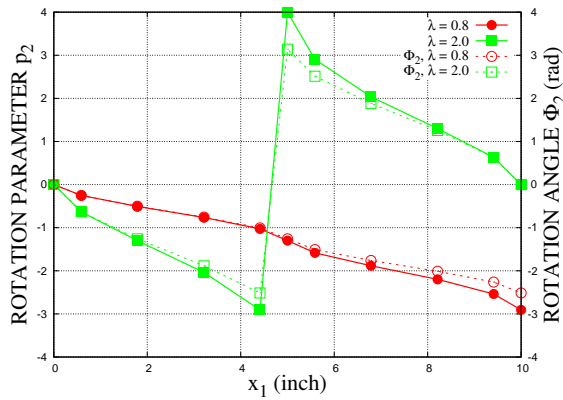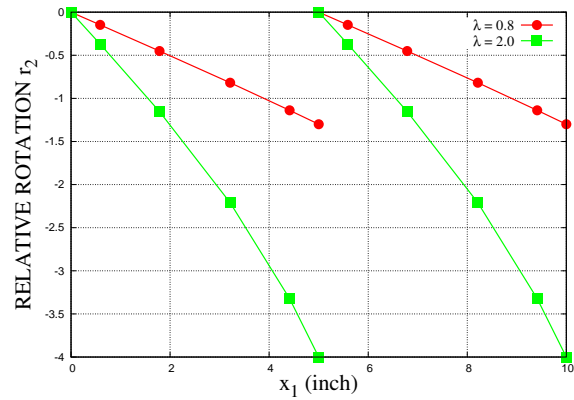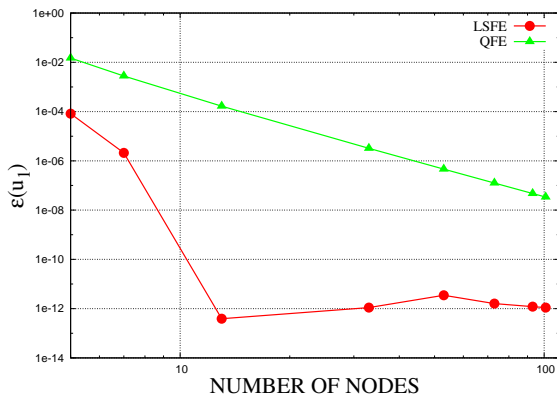
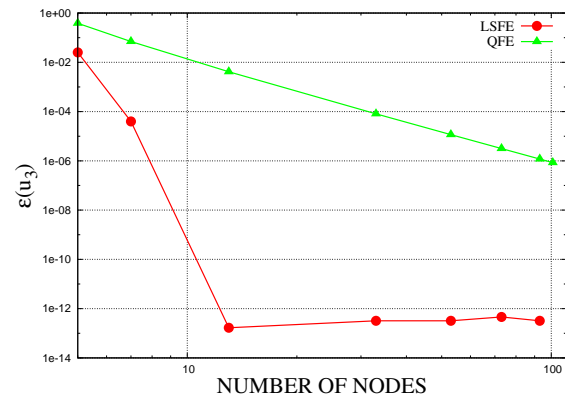(a) Rotation parameter p_2 and rotation angle ϕ_2 (b) Relative rotation r_2

Figure 5: (a) Wiener-Milenković rotation parameters and rotation angles along the beam axis x_1 as calculated by BeamDyn for two tip moments; (b) relative rotations in the two elements.

(a) u_1 (b) u_3

Figure 6: Normalized error of the (a) u_1 and (b) u_3 tip displacements of a cantilever beam (Figure 3) under constant tip moment ($\lambda = 1.0$) as a function of the total number of nodes. Results were calculated with BeamDyn (LSFE) and Dymore (QFE). LSFE model refinement was accomplished by increasing polynomial order and QFE model refinement was accomplished by increasing the number of elements.

Table 2: Numerically determined tip displacements and rotation parameters of a composite beam in Example 2 as calculated by BeamDyn (LSFE) and Dymore (QFE)

	u_1 (inch)	u_2(inch)	u_3(inch)	p_1	p_2	p_3
BeamDyn	-0.09064	-0.06484	1.22998	0.18445	-0.17985	0.00488
Dymore	-0.09064	-0.06483	1.22999	0.18443	-0.17985	0.00488

Yu et al.[33]. Readers are referred to Figure 3 for a schematic of the cantilever beam. The stiffness matrix is given as

$$C^* = 10^3 \times \begin{bmatrix} 1368.17 & 0 & 0 & 0 & 0 & 0 \\ 0 & 88.56 & 0 & 0 & 0 & 0 \\ 0 & 0 & 38.78 & 0 & 0 & 0 \\ 0 & 0 & 0 & 16.96 & 17.61 & -0.351 \\ 0 & 0 & 0 & 17.61 & 59.12 & -0.370 \\ 0 & 0 & 0 & -0.351 & -0.370 & 141.47 \end{bmatrix} \quad (37)$$

A concentrated dead force $P_3 = 150$ lbs along the x_3 direction is applied at the free tip. In the BeamDyn analysis, the beam is meshed with two 5th-order elements. The displacements and rotation parameters at each node along the beam axis are plotted in Figure 7. It is noted that the coupling effects exist between twist and the two bending modes. The applied in-plane force leads to a fairly large twist angle due to the bend-twist coupling, which can be observed in Figure 7b.

(a) *Displacements*
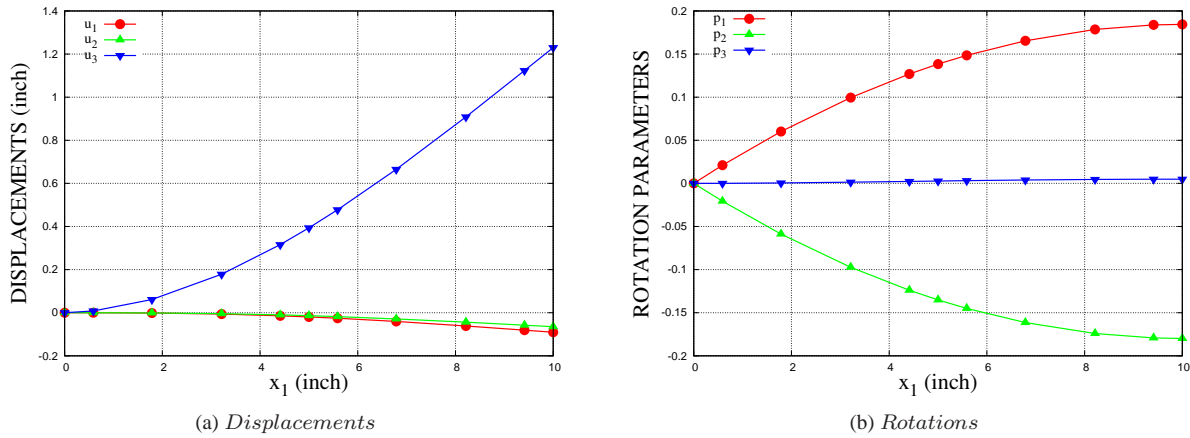
(b) *Rotations*

Figure 7: Displacements and rotation parameters along beam axis for Example 2.

The tip displacements and rotations are compared with those obtained by Dymore in Table 2 for verification, where the beam is meshed with 10 3rd-order elements. Good agreement can be observed between BeamDyn and Dymore results.

C. Example 3: Dynamic analysis of a composite beam under sinusoidal force at the tip

The last example is a transient analysis of a composite beam with boxed cross-section; the beam has the same geometry and boundary conditions as that of the previous example. The mass sectional properties are given by VABS [33,34] as

$$M^* = 10^{-2} \times \begin{bmatrix} 8.538 & 0 & 0 & 0 & 0 & 0 \\ 0 & 8.538 & 0 & 0 & 0 & 0 \\ 0 & 0 & 8.538 & 0 & 0 & 0 \\ 0 & 0 & 0 & 1.4433 & 0 & 01 \\ 0 & 0 & 0 & 0 & 0.40972 & 0 \\ 0 & 0 & 0 & 0 & 0 & 1.0336 \end{bmatrix} \quad (38)$$

The units associated with the mass matrix values are M_{ii}^* (lb s^2/in^2) and $M_{i+3,i+3}^*$ (lb s^2) for $i = 1, 2, 3$. Similarly to the C^* matrix in Example 1, the sectional mass matrix $\underline{\mathcal{M}}$ resolved in the inertial basis can be obtained by $\underline{\mathcal{M}} = (\underline{R}\,\underline{R}_0)\underline{M}^*(\underline{R}\,\underline{R}_0)^T$. The beam is divided into two 5th-order elements in the current calculation and a sinusoidal point dead force is applied at the free tip in the x_3 direction given as

$$P_3 = A_F \sin(\omega_F t) \quad (39)$$

American Institute of Aeronautics and Astronautics

where $A_F = 1.0 \times 10^2$ lbs and $\omega_F = 10$ rad/s (see Figure 8). The spectral radius ρ_∞ is set to 0.0 in the time integrator so that high frequency numerical dissipation can be achieved. The tip displacement and rotation histories of the beam are plotted in Figure 9, where the time step was 0.005 s. Note that all of the components, including three displacements and three rotations, are non-zero due to the elastic-coupling effects. The time histories of the stress resultants at the root of the beam are given in Figure 10.
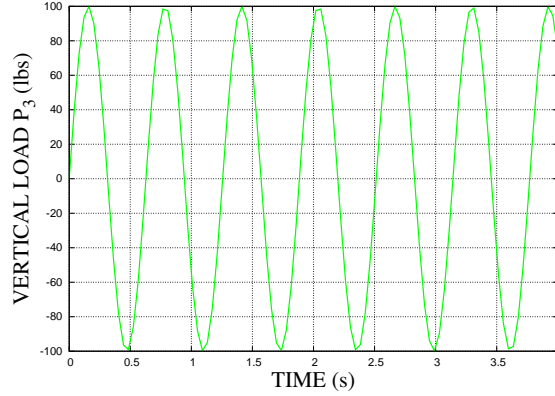
Figure 8: The applied sinusoidal vertical force at the tip in Example 3 .

Finally, we examine here the convergence rates of the LSFEs and conventional quadratic elements (in Dymore). Figure 11 shows normalized root-mean-square (RMS) error of the numerical solutions for the displacement u_1 at the free tip over the time interval $0 \leq t \leq 4$. Normalized RMS error for n_{max} numerical response values u_1^n, where $u_1^n \approx u_1(t^n)$, was calculated as

$$\varepsilon_{\text{RMS}}(u_1) = \sqrt{\frac{\sum_{k=0}^{n_{max}} \left[u_1^k - u_b(t^k) \right]^2}{\sum_{k=0}^{n_{max}} \left[u_b(t^k) \right]^2}} \tag{40}$$

where $u_b(t)$ is the benchmark solution; here $u_b(t)$ is a highly resolved numerical solution obtained by BeamDyn with one 20th-order element and the time increment was $\Delta t_b = 1.0 \times 10^{-4}$ s. Two time-increment sizes are examined in the test calculations: $\Delta t_1 = 5.0 \times 10^{-3}$ s and $\Delta t_2 = \frac{\Delta t_1}{2}$. The following observations can be made from Figure 11:

- For a fixed Δt, both Dymore (QFEs) and BeamDyn (LSFEs) converge with spatial refinement to the same error level. BeamDyn is converged with only five nodes, whereas Dymore requires at least nine nodes.

- The converged error levels are due exclusively to time-discretization error. We note that the converged error for $\Delta t_2 = \Delta t_1/2$ is one-fourth that for Δt_1, which is expected for our second-order-accurate time integrator.

V.   Conclusion

This paper presents a displacement-based implementation of geometrically exact beam theory for three-dimensional nonlinear elastic deformation. Legendre spectral finite elements are adopted for spatial discretization of the beam. Numerical examples were presented that demonstrate the capability of BeamDyn, a LSFE beam solver for wind turbine analysis developed at NREL. A benchmark static problem for nonlinear deformation of a beam was studied first. The agreement between the results calculated by BeamDyn and the analytical solution are excellent. Moreover, a convergence study was conducted, where the convergence rate of Legendre spectral elements were compared with conventional quadratic finite elements. Exponential convergence rates were observed as expected for this type of element. A composite cantilever beam was studied both statically and dynamically. The static results are verified against those obtained by Dymore. The elastic coupling effects were shown in these two cases. It concludes that BeamDyn is a powerful tool for composite beam analysis that can be used as a wind turbine blade module in the FAST modularization framework. Future work will involve more verification and validation of BeamDyn and coupling of BeamDyn to FAST, with completion expected in June 2014.
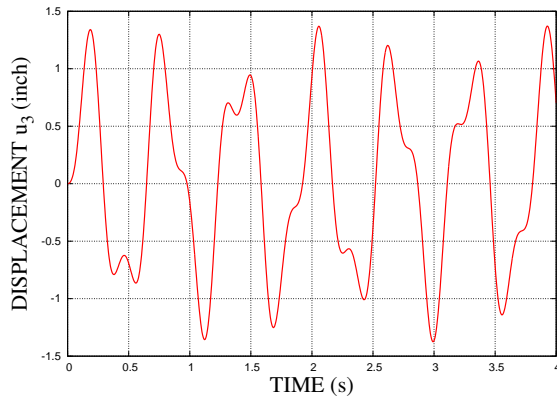
Acknowledgments

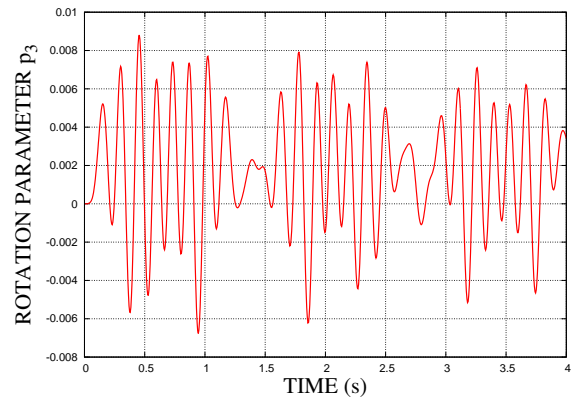American Institute of Aeronautics and Astronautics
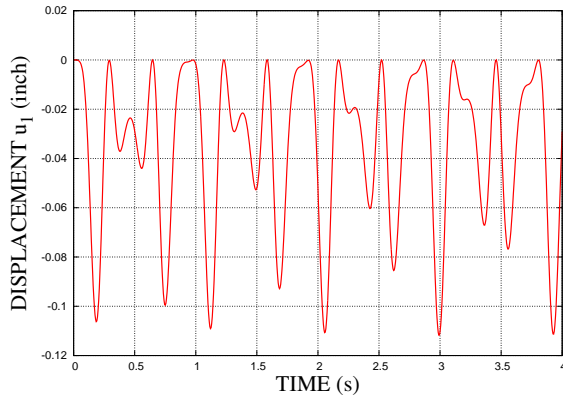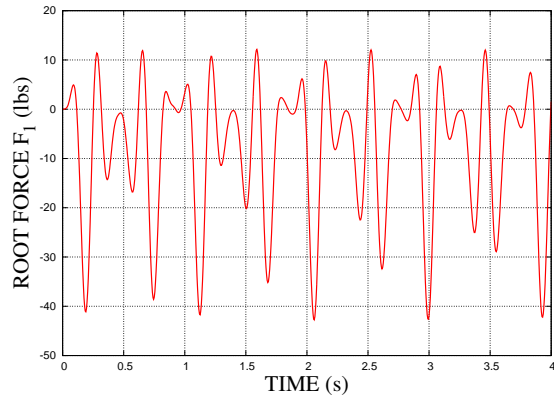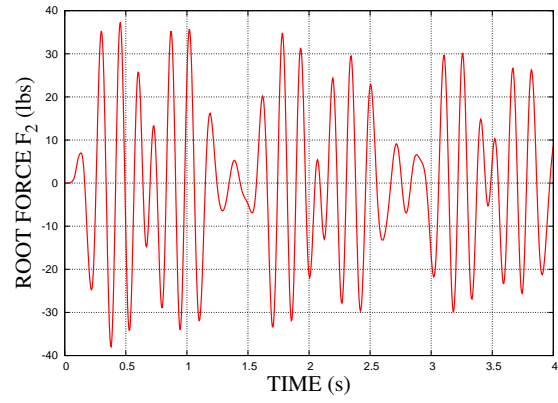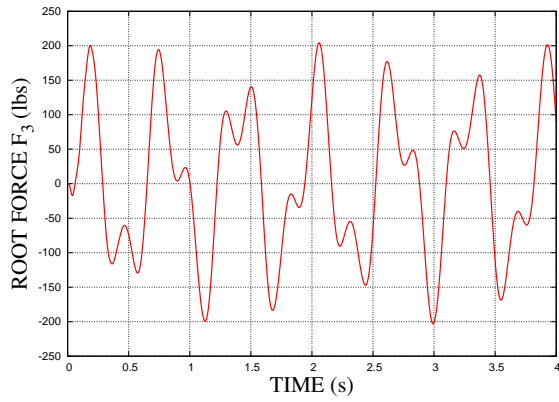
(a) u_1
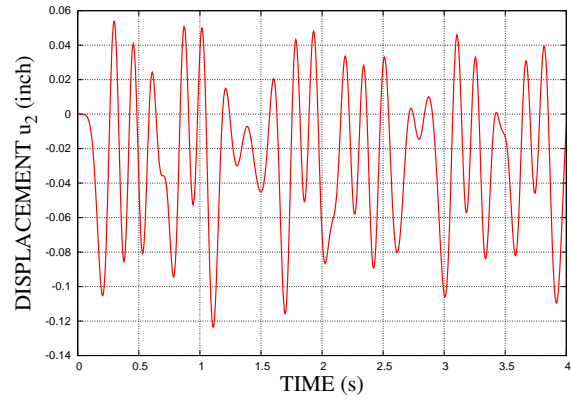
(b) u_2

(c) u_3
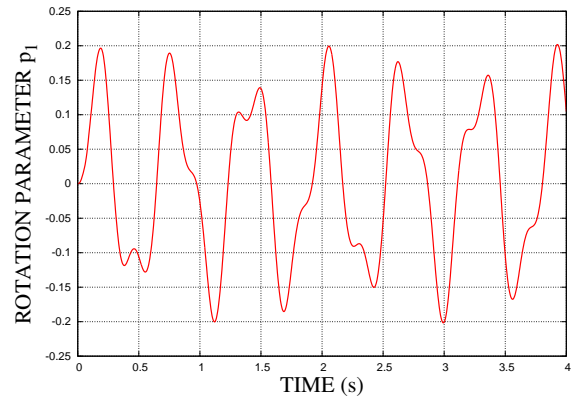
(d) p_1
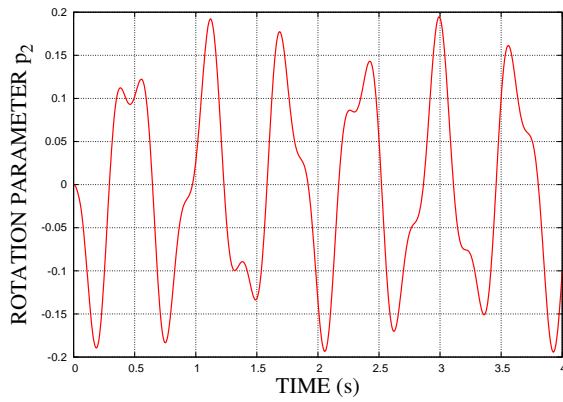
(e) p_2

(f) p_3

Figure 9: Tip displacement and rotation histories of a composite beam under vertical load.

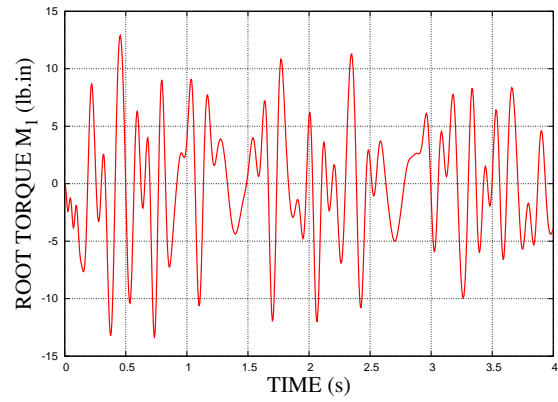American Institute of Aeronautics and Astronautics
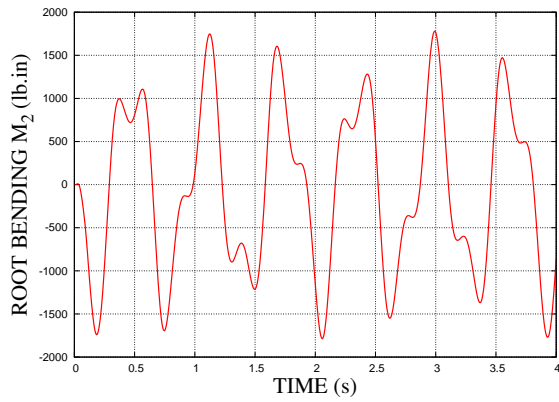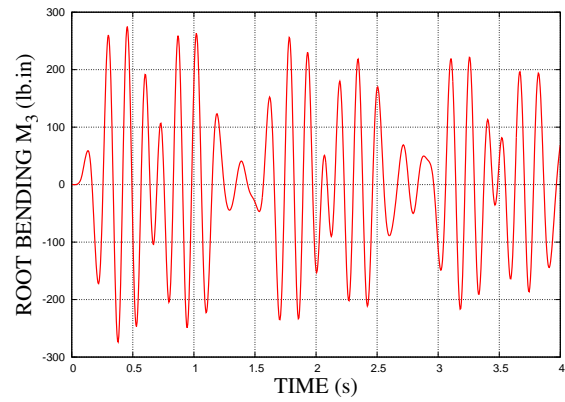
(a) F_1

(b) F_2

(c) F_3

(d) M_1

(e) M_2

(f) M_3

Figure 10: Stress resultant time histories at the root of a composite beam.
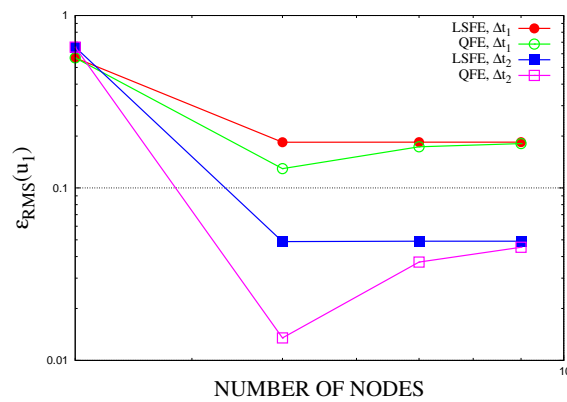
Figure 11: Normalized RMS error of tip displacement u_1 histories over $0 \le t \le 4$ as a function of number of nodes as calculated by BeamDyn (LSFEs) and Dymore (QFEs).

References

[1] Reissner, E., "On one-dimensional large-displacement finite-strain beam theory," *Studies in Applied Mathematics LII*, 1973, pp. 87–95.

[2] Simo, J. C., "A finite strain beam formulation. The three-dimensional dynamic problem. Part I," *Computer Methods in Applied Mechanics and Engineering*, Vol. 49, 1985, pp. 55–70.

[3] Simo, J. C. and Vu-Quoc, L., "A three-dimensional finite-strain rod model. Part II," *Computer Methods in Applied Mechanics and Engineering*, Vol. 58, 1986, pp. 79–116.

[4] Jelenić, G. and Crisfield, M. A., "Geometrically exact 3D beam theory: implementation of a strain-invariant finite element for statics and dynamics," *Computer Methods in Applied Mechanics and Engineering*, Vol. 171, 1999, pp. 141–171.

[5] Betsch, P. and Steinmann, P., "Frame-indifferent beam finite elements based upon the geometrically exact beam theory," *International Journal for Numerical Methods in Engineering*, Vol. 54, 2002, pp. 1775–1788.

[6] Ibrahimbegović, A., "On finite element implementation of geometrically nonlinear Reissner's beam theory: three-dimensional curved beam elements," *Computer Methods in Applied Mechanics and Engineering*, Vol. 122, 1995, pp. 11–26.

[7] Ibrahimbegović, A. and Mikdad, M. A., "Finite rotations in dynamics of beams and implicit time-stepping schemes," *International Journal for Numerical Methods in Engineering*, Vol. 41, 1998, pp. 781–814.

[8] Yu, W. and Blair, M., "GEBT: A general-purpose nonlinear analysis tool for composite beams," *Composite Structures*, Vol. 94, 2012, pp. 2677–2689.

[9] Wang, Q., Yu, W., and Sprague, M. A., "Geometric nonlinear analysis of composite beams using Wiener-Milenković parameters," *Proceedings of the 54th AIAA/ASME/ASCE/AHS/ASC Structures, Structural Dynamics, and Materials Conference*, Boston, Massachusetts, April 2013.

[10] Hodges, D. H., *Nonlinear Composite Beam Theory*, AIAA, 2006.

[11] Patera, A. T., "A spectral element method for fluid dynamics: Laminar flow in a channel expansion," *Journal of Computational Physics*, Vol. 54, 1984, pp. 468–488.

[12] Ronquist, E. M. and Patera, A. T., "A Legendre spectral element method for the Stefan problem," *International Journal for Numerical Methods in Engineering*, Vol. 24, 1987, pp. 2273–2299.

[13] Deville, M. O., Fischer, P. F., and Mund, E. H., *High-order Methods for Incompressible Fluid Flow*, Cambridge University Press, 2002.

[14] Komatitsch, D. and Vilotte, J. P., "The spectral element method: and efficient tool to simulate the seismic response of 2D and 3D geological structures," *Bulletin of the Seismological Society of America*, Vol. 88, 1998, pp. 368–392.

[15] Sridhar, R., Chakraborty, A., and Gopalakrishnan, S., "Wave propagation in anisotropic and inhomogeneous untracked and cracked structures using the pseudo spectral finite element method," *International Journal of Solids and Structures*, Vol. 43, 2006, pp. 4997–5031.

[16] Sprague, M. A. and Geers, T. L., "A spectral-element method for modeling cavitation in transient fluid-structure interaction," *International Journal for Numerical Methods in Engineering*, Vol. 60, 2004, pp. 2467–2499.

[17] Ben-Tal, A., Bar-Yoseph, P. Z., and Flashner, H., "Optimal maneuver of a flexible arm by space-time finite element method," *Journal of Guidance, Control, and Dynamics*, Vol. 18, 1995, pp. 1459–1462.

[18] Ben-Tal, A., Bar-Yoseph, P. Z., and Flashner, H., "Space-time spectral element method for optimal slewing of a flexible beam," *International Journal for Numerical Methods in Engineering*, Vol. 39, 1996, pp. 3101–3121.

[19] Kudela, P., Krawczuk, M., and Ostachowicz, W., "Wave propagation modeling in 1D structures using spectral finite elements," *Journal of Sound and Vibration*, Vol. 300, 2007, pp. 88–100.

[20] Sprague, M. A. and Geers, T. L., "Legendre spectral finite elements for structural dynamics analysis," *Communications in Numerical Methods in Engineering*, Vol. 24, 2008, pp. 1953–1965.

[21] Wang, Q. and Sprague, M. A., "A Legendre spectral finite element implementation of geometrically exact beam theory," *Proceedings of the 54th AIAA/ASME/ASCE/AHS/ASC Structures, Structural Dynamics, and Materials Conference*, Boston, Massachusetts, April 2013.

[22] Zrahia, U. and Bar-Yoseph, P., "Plate spectral elements based upon Reissner-Mindlin theory," *International Journal for Numerical Methods in Engineering*, Vol. 38, 1995, pp. 1341–1360.

[23] Kudela, P., Zak, A., Krawczuk, M., and Ostachowicz, W., "Modeling of wave propagation in composite plates using the time domain spectral element method," *Journal of Sound and Vibration*, Vol. 302, 2007, pp. 728–745.

[24] Brito, K. D. and Sprague, M. A., "Reissner-Mindlin Legendre spectral finite elements with mixed reduced quadrature," *Finite Elements in Analysis and Design*, Vol. 58, 2012, pp. 74–83.

[25] Xiao, N. and Zhong, H., "Non-linear quadrature element analysis of planar frames based on geometrically exact beam theory," *International Journal of Non-Linear Mechanics*, Vol. 47, 2012, pp. 481–488.

[26] Jonkman, J. M., "The new modularization framework for the FAST wind turbine CAE tool," *Proceedings of the 51st AIAA Aerospace Sciences Meeting including the New Horizons Forum and Aerospace Exposition*, Grapevine, Texas, January 2013.

American Institute of Aeronautics and Astronautics

[27]Bauchau, O. A., *Flexible Multibody Dynamics*, Springer, 2010.

[28]Bauchau, O., Epple, A., and Heo, S., "Interpolation of finite rotations in flexible multibody dynamics simulations," *Proceedings of the Institution of Mechanical Engineers, Part K: Journal of Multi-body Dynamics*, Vol. 222, 2008, pp. 353–366.

[29]Bathe, K. J. and Cimento, A. P., "Some pratical procedures for the solution of nonlinear finite element equations," *Computer Methods in Applied Mechanics and Engineering*, Vol. 22, 1980, pp. 59–85.

[30]Chung, J. and Hulbert, G. M., "A time integration algorithm for structural dynamics with improved numerical dissipation: the generalized-α method," *Journal of Applied Mechanics*, Vol. 60, 1993, pp. 371–375.

[31]Mayo, J. M., García-Vallejo, D., and Domínguez, J., "Study of the geometric stiffening effect: comparison of different formulations," *Multibody System Dynamics*, Vol. 11, 2004, pp. 321–341.

[32]Bauchau, O. A., "Dymore User's Manual," 2013, http://dymoresolutions.com/dymore4_0/UsersManual/UsersManual.html.

[33]Yu, W., Hodges, D. H., Volovoi, V., and Cesnik, C. E. S., "On Timoshenko-Like modeling of initially curved and twisted composite beams," *International Journal of Solids and Structures*, Vol. 39, 2002, pp. 5101–5121.

[34]Wang, Q. and Yu, W., "Asymptotic multi physics modeling of composite slender structures," *Smart Materials and Structures*, Vol. 21, 2012, pp. 035002.

American Institute of Aeronautics and Astronautics